

The Basal Stress Distribution of Ice Stream E, Antarctica, Inferred by Control Methods

DOUGLAS R. MACAYEAL

Department of Geophysical Sciences, University of Chicago, Chicago, Illinois

The irregular spatial distribution and velocity independence of basal friction derived from Landsat measured surface velocity suggests that ice stream flow is not controlled by the properties of a deformable basal till alone. Rigid bedrock substrata may contact the base of the ice stream in small (<100 km²) areas where the velocity field displays strong vorticity and where the ice stream surface appears rumbled in Landsat images.

INTRODUCTION

Satellite imagery allows precision measurement of surface velocity over regions of the Antarctic ice sheet that are heavily crevassed and therefore inaccessible by ground or air transportation. As a result, the detailed study of ice streams is now more practical and will contribute to a better understanding of the climatic evolution of the Antarctic ice sheet. In this study, I use velocity derived from Landsat Thematic Mapper imagery [Bindschadler and Scambos, 1991] to determine a subglacial friction distribution for ice stream E, Antarctica (Figure 1). This determination is motivated by the need to identify the dynamic controls on ice stream flow, and by the hypothesis that ice streams glide across thin layers of deformable basal sediment [Alley et al., 1987]. (See Engelhardt et al. [1990] for the description of a deformable sediment below ice stream B.)

Another goal of my study is to derive the distribution of subglacial friction using control methods. These methods have recently become popular for solving inverse problems involving the flow of the atmosphere and ocean (see, for example, Wunsch [1988] and Thacker and Long [1988]). Here, I introduce their application to the inverse problems associated with the interpretation of ice stream flow.

The portion of ice stream E treated in this study (Figure 1) is the 57 km by 71 km region studied by Bindschadler and Scambos [1991]. They compared Landsat images taken at different times and were able to determine the surface velocity from the displacement of various visible features (Figure 2). The study region lies about midway along the course of ice stream E. Its most conspicuous visible features are the ice stream margins and the faint lineations which align with the flow (Figure 1a). The linear series of surface undulations that intersect the Southern edge of the ice stream suggest flow over rigid bedrock topography, and will be shown here to correlate with strong basal friction.

Ice thickness and surface elevation over the study region (Figure 3) are interpolated from large-scale contour maps compiled by Drewry [1983]. Although not as well quantified as the surface velocity, pressure gradients associated with surface undulations evident in the Landsat image (Figure 1a) are unlikely to be the primary cause of the velocity variations seen in Figure 2. This is because gradients have zero curl. Basal friction alone is able to produce the curl of the observed

velocity evident in Figure 4. This is why I focus on determining the regional variation of basal friction.

ICE STREAM DYNAMICS

Given an ice thickness H , a surface elevation z_s , a basal friction coefficient β , and flow law parameters B and n , the horizontal velocity $U=(u,v)$ is the solution of the following the depth-integrated stress equilibrium equations [MacAyeal, 1989],

$$\frac{\partial}{\partial x} \left[2\nu H \left(2\frac{\partial u}{\partial x} + \frac{\partial v}{\partial y} \right) \right] + \frac{\partial}{\partial y} \left[\nu H \left(\frac{\partial u}{\partial y} + \frac{\partial v}{\partial x} \right) \right] - \beta^2 u - \rho g H \frac{\partial z_s}{\partial x} = 0 \quad (1)$$

$$\frac{\partial}{\partial y} \left[2\nu H \left(2\frac{\partial v}{\partial y} + \frac{\partial u}{\partial x} \right) \right] + \frac{\partial}{\partial x} \left[\nu H \left(\frac{\partial u}{\partial y} + \frac{\partial v}{\partial x} \right) \right] - \beta^2 v - \rho g H \frac{\partial z_s}{\partial y} = 0 \quad (2)$$

Notation is explained at the end of the paper. The depth average viscosity ν is strain rate dependent and accounts for steady state power law creep [Thomas and MacAyeal, 1982],

$$\nu = \frac{B}{2 \left[\left(\frac{\partial u}{\partial x} \right)^2 + \left(\frac{\partial v}{\partial y} \right)^2 + \frac{1}{4} \left(\frac{\partial u}{\partial y} + \frac{\partial v}{\partial x} \right)^2 + \frac{\partial u}{\partial x} \frac{\partial v}{\partial y} \right]^{\frac{n-1}{2n}}} \quad (3)$$

Horizontal velocity components u and v are independent of the vertical coordinate z and are thus first-order approximations to the horizontal velocity at the surface of the ice stream.

Equations (1) and (2) are approximations to the full, three-dimensional stress equilibrium equations. They are valid when the ratio of thickness to horizontal span of the ice stream is small and when the basal friction is small compared to the stress needed to induce significant vertical shear. A derivation of these equations using asymptotic expansions in terms of nondimensional parameters is provided by MacAyeal [1989]. The best indication that these equations apply to ice stream E is the fast basal ice velocity apparent in the Landsat images

Copyright 1992 by the American Geophysical Union.

Paper number 91JB02454.
0148-0227/92/91JB-02454\$05.00

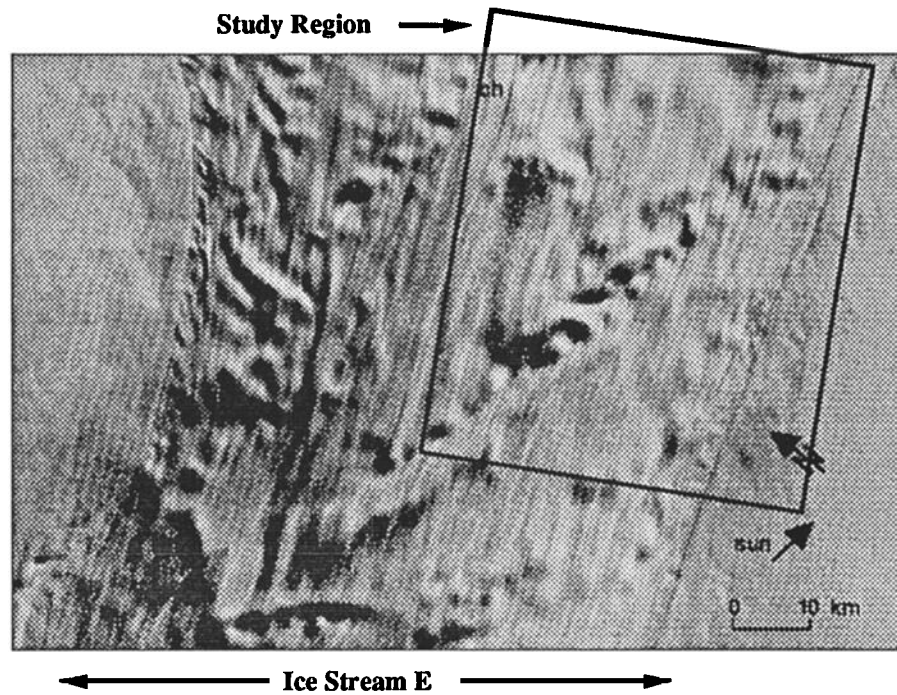


Fig. 1a. Landsat image of ice stream E, West Antarctica, showing the study region [Bindschadler and Scambos, 1991; Stephenson and Bindschadler, 1990]. The ice stream interior is rumpled by fast, depth independent flow across bedrock undulations. Ice motion in areas outside the ice stream is imperceptible and probably falls below 20 m/yr. The boxed region denotes the study area where the basal friction was determined using surface velocity observations.

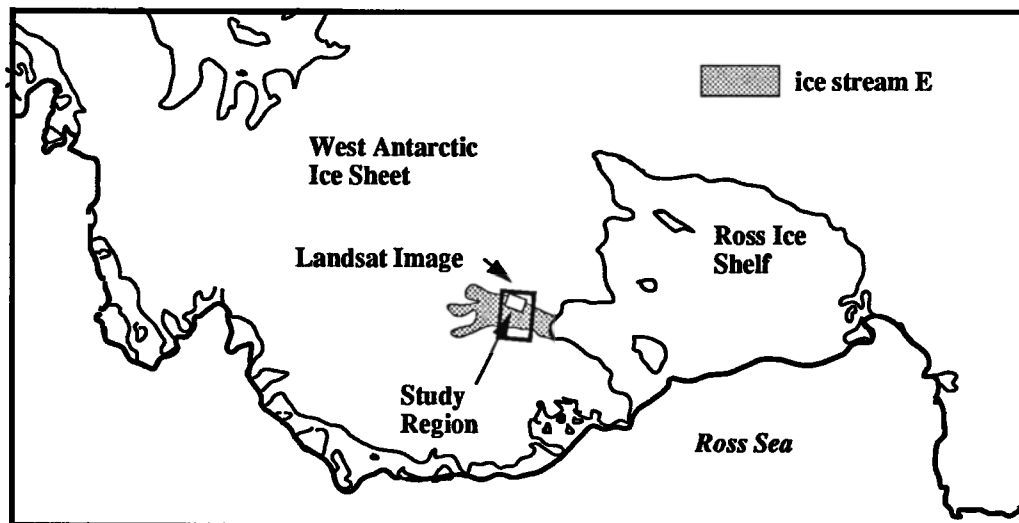


Fig. 1b. Location map of West Antarctica. The Landsat image shown in Figure 1a covers a small portion of ice stream E located approximately midway between its head and the grounding line of the Ross Ice Shelf. Ice stream B, which has been shown to glide on a deformable subglacial sediment, is located south of ice stream E and also discharges into the Ross Ice Shelf.

[Bindschadler and Scambos, 1991; Stephenson and Bindschadler, 1990]. These images suggest that surface rumpling is caused by fast basal flow over small-scale bedrock topography (Figure 1). Such undulations are generally not visible where the ice is frozen to a rigid bed.

Basal friction is represented by the $\beta^2 u$ and $\beta^2 v$ terms in (1) and (2). In this representation, two physical assumptions are imposed. First, the friction is assumed to be parallel to the direction of the depth-averaged horizontal ice velocity. Second, the basal friction coefficient β^2 is assumed positive definite. These restrictions ensure that basal drag represents a sink to the mechanical energy of the ice stream at all points.

Flow law parameters B and n are assumed to be $1.73 \times 10^8 \text{ Pa s}^{1/3}$ and 3 (nondimensional units), respectively. The constant B

is determined by the temperature depth profile of the ice stream and accounts for the depth-integrated stiffness of the ice column when sustaining depth independent horizontal strain rate. Its value was computed from the temperature dependent function recommended by Thomas and MacAyeal [1982] using a temperature depth profile observed at ice stream B [Engelhardt et al., 1990]. A temperature depth profile of ice stream E is not available. The similarity of the two ice streams, and the proximity of their location with respect to Antarctic surface climate patterns, suggests that the ice stream B profile should be a reasonable approximation to that of ice stream E.

Boundary conditions associated with (1) and (2) can be either dynamic or kinematic. In the former case, vertically

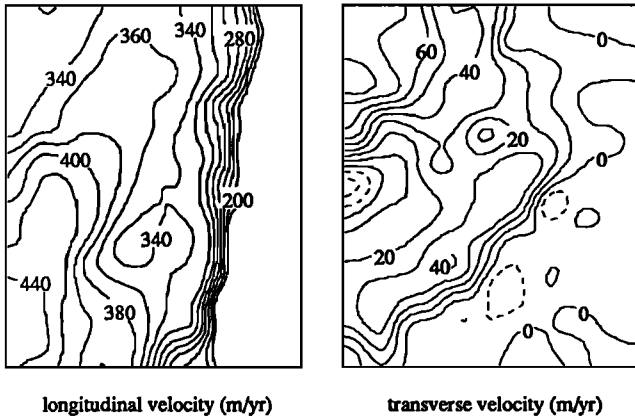


Fig. 2. Longitudinal and transverse components of the surface velocity field observed by *Bindschadler and Scambos* [1991]. The longitudinal direction is defined to be parallel to the south edge of the ice stream visible in Figure 1a and towards the bottom of the map. (This edge trends approximately 10° off the side of the rectangular study region.) These data are interpolated by *Bindschadler and Scambos* [1991] from 248 irregularly distributed observation points using a commercially available software package based on kriging principles. Smoothing to correct for obvious artifacts of the interpolation procedure was done by hand [*Bindschadler and Scambos*, 1991].

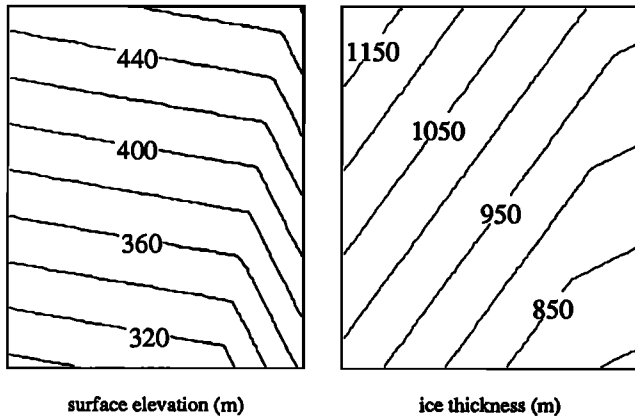


Fig. 3. Ice thickness (right) and surface elevation (left). These fields were estimated from Antarctic Folio Series maps [*Drewry*, 1983] which present the large-scale ice geometry. Accuracy is estimated to be approximately 100 m for ice thickness and 50 m for surface elevation.

integrated stresses are specified. In the latter case, U is specified. In the present study, it is most convenient to specify kinematic conditions at all boundaries of the study region. This is because the boundaries do not lie on natural breaks in the system where the vertically integrated stresses can be specified. To specify the kinematic boundary conditions required for the solution of (1)-(3), I set both components of U equal to the Landsat image derived velocity provided by *Bindschadler and Scambos* [1991].

INVERSE PROBLEM

The goal of this study is to determine the distribution of $\beta(x,y)$ from a known distribution of the surface velocity denoted $U_d(x,y)$ (shown in Figure 2). As mentioned previously, the strong variations of $\nabla \times U_d$ seen in Figure 4 substantiate the expectation that $\beta(x,y)$ is the primary cause of the observed surface velocity variations.

There are two approaches to solving the inverse problem posed above: (1) a direct approach involving algebraic

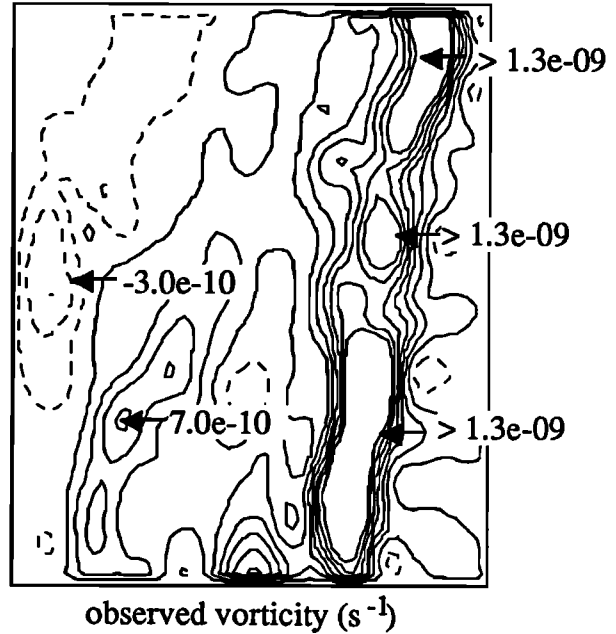


Fig. 4. $\nabla \times U_d$ (s^{-1}). Vorticity along the ice stream margin is associated with shear in the longitudinal flow. Vorticity in the interior of the ice stream is probably caused by variations in basal friction. (In this and other figures, contours are labeled using scientific notation, e.g., 3.0×10^{-10} is equivalent to 3.0×10^{-10} .)

inversion of (1) and (2), and (2) a least squares approach involving control methods and a numerical model which solves (1) and (2) when given a trial β field. I describe the direct inversion first because it is simple and therefore preferred if conditions permit its use.

In brief, the direct algebraic inversion is accomplished by manipulation of (1) and (2) to isolate β :

$$\beta = \frac{1}{\sqrt{u_d}} \left[\frac{\partial}{\partial x} \left(2\nu H \left(2 \frac{\partial u_d}{\partial x} + \frac{\partial v_d}{\partial y} \right) \right) + \frac{\partial}{\partial y} \left(\nu H \left(\frac{\partial u_d}{\partial y} + \frac{\partial v_d}{\partial x} \right) \right) - \rho g H \frac{\partial z_s}{\partial x} \right]^{\frac{1}{2}} \quad (4)$$

or,

$$\beta = \frac{1}{\sqrt{v_d}} \left[\frac{\partial}{\partial y} \left(2\nu H \left(2 \frac{\partial v_d}{\partial y} + \frac{\partial u_d}{\partial x} \right) \right) + \frac{\partial}{\partial x} \left(\nu H \left(\frac{\partial u_d}{\partial y} + \frac{\partial v_d}{\partial x} \right) \right) - \rho g H \frac{\partial z_s}{\partial y} \right]^{\frac{1}{2}} \quad (5)$$

Variables u_d and v_d are the observed velocity components which can be substituted into the expressions above. Equations (4) and (5) are redundant and, when solved together, overdetermine β .

To solve these equations, it is necessary to evaluate the first and second partial derivatives of the observed velocity, and this requires interpolation of the irregularly distributed velocity measurements. As is well known, there are many ways to interpolate a field of irregularly spaced observations. *Bindschadler and Scambos* [1991] used a commercially available package based on kriging principles, and then adjusted the results by hand. It is thus possible for the interpolation method to artificially affect the β field derived

from (4) and (5). To avoid these effects, I recommend using an interpolation scheme that is faithful to the physics which govern the ice stream velocity. This scheme is the control method which I discuss below.

The direct algebraic inversion also faces several other mathematical hazards. It works only if the data, $U_d = (u_d, v_d)$, possess all of the mathematical properties required of a solution of (1) - (3). There may be velocity gradients contained in this data that cannot be explained by any distribution of β . In this circumstance, β determined from (4) or (5) might be complex, or (4) and (5) might give different values of β . Such problems are commonly encountered in analysis of discrete velocity measurements which require interpolation to an evenly spaced grid for the evaluation of derivatives [Frolich and Doake, 1988].

THE CONTROL METHOD

The second approach to the inverse problem stated above follows from control theory [Wunsch, 1988; Thacker and Long, 1988]. This approach is adopted here because it allows for velocity data that are incompatible with solutions of (1)-(3), and therefore circumvents the difficulties noted above. One might question whether incompatibility, if encountered, should demand an improvement of the governing equations instead of an improvement in the inverse method. As stated above, (1)-(3) are approximations to the stress equilibrium equations which are justified for large-scale, low-friction flow phenomena. Their use in studying the velocity variations of ice stream E is thus appropriate even though the velocity observations may reflect small scale phenomena which are not of interest. As a result, an appropriate inverse method is imperative in the study of large scale phenomena described by (1)-(3).

The control method differs from the direct algebraic method discussed above by not requiring the observations to be an exact solution of (1)-(3). Instead, the control method seeks a family of subglacial friction distributions which, when used in (1)-(3), give solutions that are as close as possible to the observed velocity field. To find this family, the control problem must have (1) a numerical model of the forward problem (represented by (1)-(3) with associated kinematic boundary conditions) and (2) a measure of model performance in matching the observed velocity distribution. The numerical model used here is discussed below and is based on a finite-difference implementation of the ice stream model used previously to simulate the flow of ice stream B [MacAyeal, 1989]. Model performance will be measured by the following number (referred to as the performance index):

$$\begin{aligned}
 J = & \iint_{\Gamma} \frac{1}{2} \Sigma(x,y) \left[(u - u_d)^2 + (v - v_d)^2 \right] dx dy \\
 & + \iint_{\Gamma} \lambda(x,y) \left\{ \frac{\partial}{\partial x} \left[2\nu H \left(2 \frac{\partial u}{\partial x} + \frac{\partial v}{\partial y} \right) \right] \right. \\
 & \left. + \frac{\partial}{\partial y} \left[\nu H \left(\frac{\partial u}{\partial y} + \frac{\partial v}{\partial x} \right) \right] - \beta^2 u - \rho g H \frac{\partial z}{\partial x} \right\} dx dy \\
 & + \iint_{\Gamma} \mu(x,y) \left\{ \frac{\partial}{\partial y} \left[2\nu H \left(2 \frac{\partial v}{\partial y} + \frac{\partial u}{\partial x} \right) \right] \right. \\
 & \left. + \frac{\partial}{\partial x} \left[\nu H \left(\frac{\partial u}{\partial y} + \frac{\partial v}{\partial x} \right) \right] - \beta^2 v - \rho g H \frac{\partial z}{\partial y} \right\} dx dy \quad (6)
 \end{aligned}$$

where Γ denotes the areal domain of the study region, and where $\Sigma(x,y)$ is a data-weighting function designed to account for spatial variation in the uncertainty of U_d .

The vector field $\Lambda = (\lambda, \mu)$ is introduced in (6) as a Lagrange undetermined multiplier [Bryson and Ho, 1975]. Its purpose is to enforce the satisfaction of (1) and (2) as constraints on the model U field. Equation (3) is satisfied implicitly by the ice stream model. One could equally well enforce (3) by using a Lagrange multiplier formulation. This is not done in the present study because the numerical model of the forward problem has an acceptable technique for satisfying the flow law.

As shown below, Λ represents the essence of the control method. Its introduction adds two more variables, λ and μ , to the problem, and this may be viewed as a complication. The addition is justified, however, because the two new variables indicate how corrections to a trial β field can change the misfit between model and observation.

LIMITS TO β FIELD OBSERVABILITY

The observed velocity field $U_d(x,y)$ was derived from a finite set of discrete velocity measurements [Bindshadler and Scambos, 1991]. It is thus unrealistic to expect the $\beta(x,y)$ which minimizes J to be unique or to possess an arbitrarily high spatial resolution. This opinion is reinforced by the analysis of Balise and Raymond [1985] which shows that small-scale variations in basal sliding of a linearly viscous glacier, presumably caused by variations in basal friction, are attenuated in the vertical. Assuming the analysis by Balise and Raymond [1985] to be applicable to ice streams, it leads to the conclusion that spatial variations in β with length scales less than approximately 4 times the ice thickness would not be identifiable from surface velocity.

To account for this conclusion, and for the limited degrees of freedom in the velocity measurements, I express the β field as the sum of functions which possess length scales larger than approximately 4 km:

$$\beta(x,y) = \sum_{i=1}^{903} \alpha_i F_i(x,y) \quad (7)$$

The basis functions $F_i(x,y)$ determine the accuracy and resolution of the inferred β field. If β were to satisfy some known physical constraint, then it would be prudent to select basis functions which also satisfy this constraint and which are linearly independent in their function space. The basis functions used here are composed of the products of $\sin(k\pi x/L_x)$ or $\cos(k\pi x/L_x)$ and $\sin(l\pi y/L_y)$ or $\cos(l\pi y/L_y)$, where k and l are integers ranging from 1 to 15, and $L_x = 71$ km and $L_y = 57$ km are the horizontal dimensions of the rectangular study region (Figure 1). There are 900 such functions. Linear trends in x and y , and a constant field, are also considered. This brings the total number of basis functions considered to 903.

THE GRADIENT OF THE PERFORMANCE INDEX

Having restricted the scale of β field variation, the problem reduces to determining the scalar quantities $\alpha_i, i=1, \dots, 903$. This can be done by expressing the gradient of J with respect to the α_i and by searching for a location in α space where this gradient vanishes. Using the calculus of variations, $\partial J / \partial \alpha_i$ can be derived from (6):

$$\frac{\partial J}{\partial \alpha_i} = - \iint_{\Gamma} 2F_i \left[\sum_{j=1}^{903} \alpha_j F_j(x,y) \right] (\Lambda \cdot U) dx dy \quad (8)$$

To evaluate this expression $\partial J/\partial \alpha_i$ at an arbitrary location in a space, it is necessary to form the vector product between U and Λ . The vector U is evaluated by using a numerical model to solve (1)-(3) with a trial β field. The other vector, Λ , is evaluated by solving the adjoint forms of (1) and (2) when linearized about the effective viscosity distribution used to derive U :

$$\frac{\partial}{\partial x} \left[2\nu H \left(2 \frac{\partial \lambda}{\partial x} + \frac{\partial \mu}{\partial y} \right) \right] + \frac{\partial}{\partial y} \left[\nu H \left(\frac{\partial \lambda}{\partial y} + \frac{\partial \mu}{\partial x} \right) \right] - \beta^2 \lambda = \Sigma(x,y) (u_d - u) \quad (9)$$

$$\frac{\partial}{\partial y} \left[2\nu H \left(2 \frac{\partial \mu}{\partial y} + \frac{\partial \lambda}{\partial x} \right) \right] + \frac{\partial}{\partial x} \left[\nu H \left(\frac{\partial \lambda}{\partial y} + \frac{\partial \mu}{\partial x} \right) \right] - \beta^2 \mu = \Sigma(x,y) (v_d - v) \quad (10)$$

$$\lambda = \mu = 0 \quad \text{on } \partial \Gamma \quad (11)$$

Equations (9) and (10) are generated from (6) by setting the variations of J with respect to u and v to zero. Boundary conditions are used to deduce (11). The form of (9)-(11) deserve comment. Boundary conditions are homogeneous, and the driving stress term $\rho g H \nabla z_x$ is absent. Forcing is provided only by mismatch between U and U_d . The Lagrange multiplier field can thus be interpreted as being similar to a Green's function for an ice stream forced by model/observation mismatch. The Lagrange multiplier thus serves an important role in the mathematical procedures which minimize J . It explicitly determines the influence of changes in β on mismatch between model and observation.

CONDITIONS THAT MINIMIZE J

It is instructive to consider the conditions that confirm the minimization of J . There are five possible ways to satisfy the condition that $\partial J/\partial \alpha_i = 0$ for all $i=1, \dots, 903$. First, all the α_i can be zero. This case is unlikely. Second, U can be zero. Again, this case is unlikely. Third, Λ can be zero. This case is highly desirable but rarely achieved. Given that Λ is forced only by errors in matching the observed velocity, $\Lambda=0$ would imply that the observations were matched perfectly and that the minimum of J is zero. Fourth, U and Λ can be orthogonal at all points. Fifth, and most likely, the scalar function $U \cdot \Lambda$ can be orthogonal (in the functional analysis sense) to all of the functions comprising the products of the first two factors in the integrand of (8). This is the normal circumstance encountered in the minimization of J and indicates that match between model and observation can be improved only by increasing the number of degrees of freedom in β or by eliminating errors in the observations which are incompatible with model physics.

The algorithm I use to minimize J is described as follows. I guess an initial set of scalars $\alpha_i, i=1, \dots, 903$, termed $\alpha_i^{(0)}$. Using this guess, I solve the forward problem (equations (1)-(3) with associated kinematic boundary conditions) to determine an initial U , termed $U^{(0)}$. I next solve the (9)-(11) for $\Lambda^{(0)}$ using $(U - U^{(0)})$ as the forcing. With $\Lambda^{(0)}$ so determined, I evaluate $\partial J/\partial \alpha_i, i=1, \dots, 903$, using (8). If $\partial J/\partial \alpha_i$ is not zero, or sufficiently close, I then correct the initial guess of $\alpha_i, i=1, \dots, 903$, by searching down the gradient of J using a univariate minimization algorithm (IMSL UVMIF). This correction, termed $\alpha_i^{(1)}$, is used to generate $U^{(1)}$. The $U^{(1)}$ is then treated in the same manner as $U^{(0)}$ to iteratively improve the match between model and observation.

The iterative procedure is stopped when $\partial J/\partial \alpha_i, i=1, \dots, 903$, is zero, or sufficiently close. In the present application, the iteration stops when the change of $\partial J/\partial \alpha_i, i=1, \dots, 903$, from one cycle to the next drops 3 orders of magnitude, and when further reduction would require a relatively large expenditure of additional computer time. In the present study, 75 iterations were adequate.

SATELLITE IMAGERY DERIVED VELOCITY DATA

Bindschadler and Scambos [1991] measured surface velocities at 248 points distributed irregularly across the imaged region by comparing surface features between two images acquired at different times. Displacements of these surface features over a nearly 2-year time period gave velocities accurate to about 20 m/yr or better. The irregular distribution of data points was dictated by the presence of identifiable surface features such as crevasses and surface bumps. Velocity data are thus concentrated in regions where the ice stream is heavily crevassed. This concentration is beneficial for the inversion technique because surface crevassing is often caused by strong velocity gradients [*Bindschadler et al.*, 1987].

Figure 2 shows a contour map of longitudinal and transverse components of the observed surface velocity interpolated to a 65x65 finite difference grid to be used in the modeling and inversion calculations. The longitudinal direction is taken to be downstream parallel to the ice stream edge and is positive downward in Figure 1a. The transverse direction is orthogonal to the longitudinal direction and is positive to the right in Figure 1a.

Many of the large-scale velocity patterns shown in Figure 2 are common to West Antarctic ice streams. At the ice stream margin, 75% of the maximum midchannel velocity is attained within a 5 to 10 km shear band. Within the interior of the ice stream, velocity variation is much less dramatic. The most significant variation there consists of a elongated region of reduced longitudinal velocity which intersects the edge of the ice stream at approximately 45° (Figure 2). This feature appears to be correlated with a series of surface bumps and depressions suggestive of bedrock topography (Figure 1a) as described by *Bindschadler and Scambos* [1991].

In the present circumstance, the data uncertainty weighting function $\Sigma(x,y)$ is 1 at all points within the ice stream and 0 at all points outside. This evaluation reflects the opinion that the kriging interpolation performed by *Bindschadler and Scambos* [1991] yields approximately the same degree of uncertainty within the interior of the ice stream (about 20 m/yr). *Bindschadler and Scambos* [1991] were unable to measure velocity at points exterior to the ice stream because surface features there were indistinct and displacements were imperceptible on the Landsat images. To avoid constraining the derived β field by the highly uncertain velocity extrapolated over the exterior of the ice stream, $\Sigma(x,y)$ is 0 there.

RESULTS

To invert the observed velocity for the β field, I treated (1)-(3), (6), and (9)-(11) using the finite difference method with a 65x65 grid. Grid resolutions were 1113 m and 891 m in the longitudinal and transverse directions, respectively. To constrain the modeled velocity in the region outside the ice stream, β was arbitrarily set to 4.0×10^5 (Pa s/m)^{1/2}. This was done to ensure that the modeled velocity would be close to zero (typically < 5 m/yr) outside of the apparent ice stream domain. This adjustment was made by adding a 904th function, F_{904} , to the series expansion (7). The value of F_{904} at grid points within the ice stream is 0. Outside the ice stream,

its value is $4.0 \times 10^5 \text{ (Pa s/m)}^{1/2}$. The coefficient α_{904} is 1, and was not changed during the minimization of J .

Figure 5 displays the inferred distribution of $\beta^2(x,y)$. Over most of the region, β^2 is reasonably uniform and is less than $1 \times 10^9 \text{ Pa s/m}$. This result is consistent with studies of ice stream B [Alley et al., 1987; MacAyeal, 1989]. In the neighborhood of the elongated region of reduced longitudinal velocity (Figure 2), β^2 rises in magnitudes above $8 \times 10^9 \text{ Pa s/m}$. The locations of this and other local maxima are coordinated with the surface undulations seen in Figure 1a. The existence of these relatively small scale regions of strong basal friction is consistent with previous analysis [Whillans et al., 1989] and suggests the influence of rigid subglacial bedrock topography.

The model velocity field U associated with the derived β^2 field is shown in Figure 6. The residual misfit between

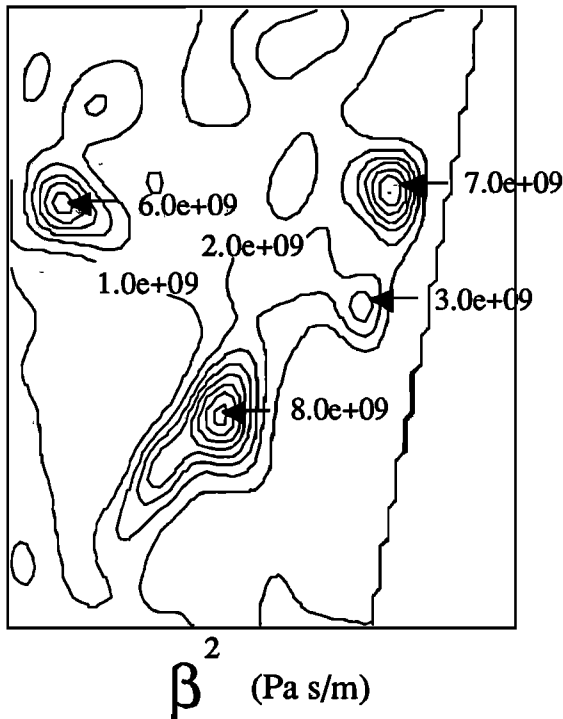


Fig. 5. Inferred distribution of the basal friction coefficient β^2 . Irregularity of this distribution suggests that basal friction is enhanced by ice contact with rigid bedrock, or by variations in subglacial water pressure. The average value of β^2 within this region is consistent with inferred friction coefficients for ice stream B [MacAyeal, 1989; Alley et al., 1987].

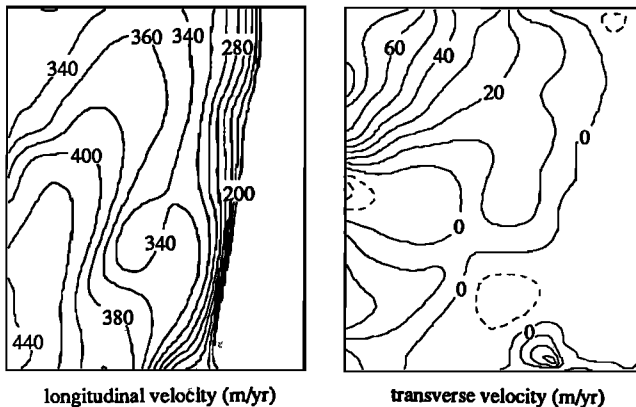


Fig. 6. Modelled velocity which best fits data using the basal friction coefficient shown in Figure 5.

modeled and observed surface velocity is shown in Figure 7. After 75 iterations of the minimization algorithm described previously, the average disagreement between modeled and observed velocity falls below 12 m/yr. The modeled velocity thus agrees with the observed velocity well within the uncertainty of the observations. Disagreement is largest at the ice stream margin and where strong surface undulations are seen in Figure 1a. In the first case, the simplified treatment of the ice temperature and rheological properties in the model may preclude a better fit to the observations. In the second case, bedrock topography, the presumed cause of the surface undulations, may introduce small-scale vertical shear stresses not allowed by (1)-(3) [MacAyeal, 1989].

As a cursory interpretation of the inferred subglacial friction, I display in Figure 8 contour maps of the components of the basal friction ($\beta^2 u, \beta^2 v$). Figure 9 displays the ratio of the assumed driving stress to basal friction in the longitudinal direction. As indicated by the surface elevation shown in Figure 3, the assumed driving stress is directed longitudinally within the ice stream. Figure 9 indicates that the driving stress predominantly exceeds the basal friction along the ice stream margin where horizontal shear stresses tend to retard the longitudinal flow. This observation is consistent with the fact that horizontal deviatoric stresses play an important role in the force balance [MacAyeal, 1989].

Figure 9 also shows the curl of the derived basal friction ($\nabla \times (\beta^2 U)$). The assurance that basal friction is the cause of the observed velocity variations is the fact that driving stress $-\rho g(z_s - z_b) \nabla z_s$, where z_b is the elevation of the ice/bed

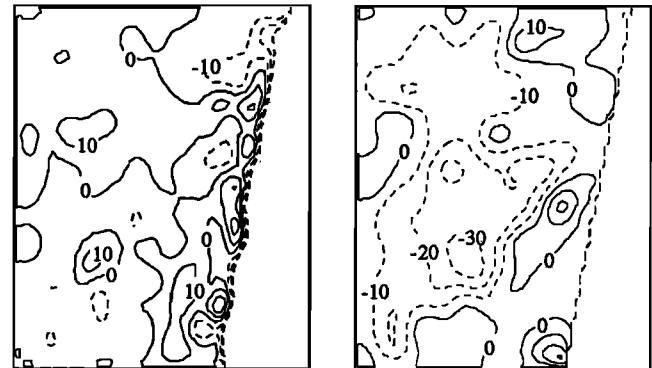


Fig. 7. $U - U_d$ (see Figures 2 and 6).

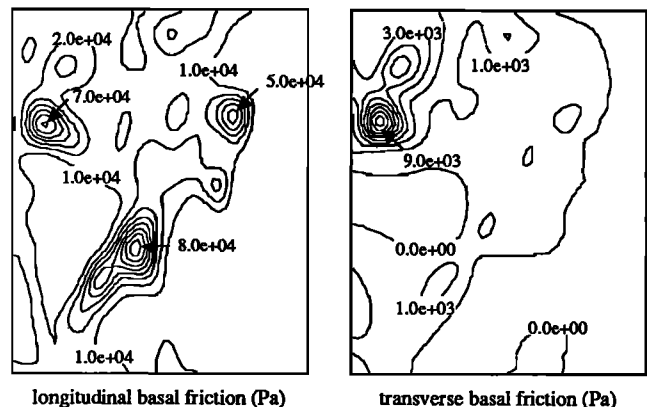


Fig. 8. Basal friction per unit area, $\beta^2 U$, resolved into longitudinal (left) and transverse (right) components.

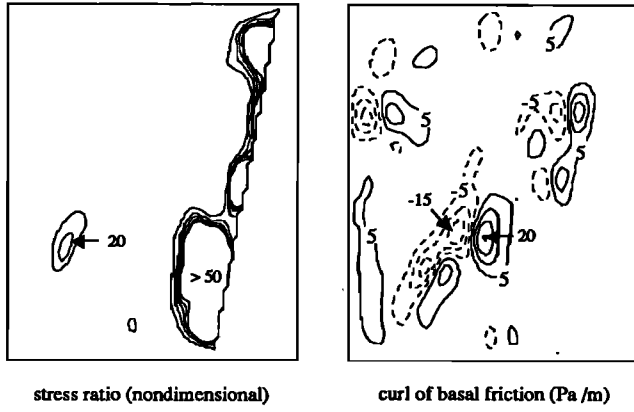


Fig. 9. Ratio of longitudinal driving force per unit area to the longitudinal component of the basal friction per unit area (left). A similar ratio for transverse components is zero within the ice stream interior because, according to the assumed surface topography shown in Figure 3, there is no transverse surface slope within the ice stream. The curl of the basal friction per unit area (right). This curl suggests that surface undulations could not serve equally well as basal friction in accounting for the observed velocity.

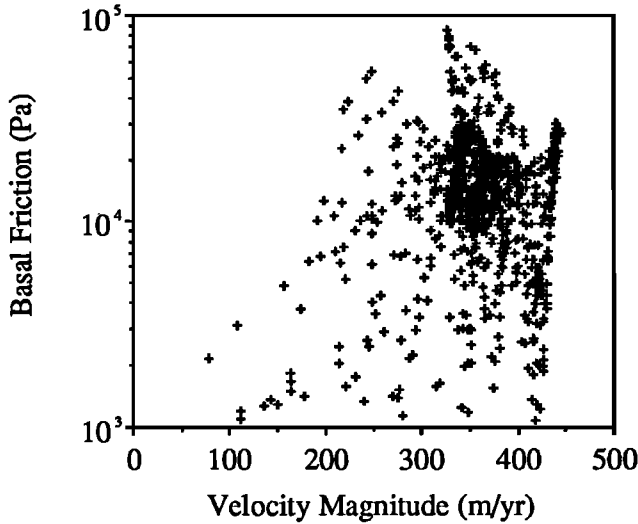


Fig. 10. Scatter plot of $|\beta^2 U|$ versus $|U|$. Individual points represent results at grid points in the finite difference model. A lack of correlation suggests that the subglacial bed is not characterized by a deformable sediment having constant viscosity and thickness.

contact, cannot have curl comparable to that shown in Figure 9. To have comparable curl, z_b would have to have slopes in excess of 1 to 1 over large horizontal distances. This is clearly unrealistic [Drewry, 1983].

To examine the rheological properties of the subglacial bed, a plot of the inferred basal shear stress at each grid point, $|\beta^2 U|$, as a function of the velocity magnitude at each grid point, $|U|$, is shown in Figure 10. No relationship is seen; and this suggests that basal friction is more determined by position than by local ice velocity. This result argues against the existence of a deforming subglacial sediment with uniform viscosity and thickness. It is consistent, however, with the possibility that a deformable subglacial layer exists, but does not possess uniform thickness or viscosity.

UNCERTAINTY

Uncertainty of the inferred β field derived above can come from many sources. The most serious source examined here is

the fact that surface elevation is determined from a large-scale map [Drewry, 1983] which does not resolve features on a scale as small as the inferred variation in β . This uncertainty gives rise to the question of whether variation of surface topography could produce equally well the observed surface velocity field as the basal friction inferred above.

To answer this question, I solved for the surface elevation field $z(x,y)$ that would reproduce the observed surface velocity when β is assumed constant. In deriving $z(x,y)$, I chose to hold $H(x,y)$ constant as shown in Figure 3. The variations of z are thus assumed to be caused by the basal topography on which the ice stream rests.

As with the inference of β , the determination of $z(x,y)$ from surface velocity data may also present mathematical hazards. In a direct algebraic inversion comparable to (4) and (5), for example, expressions for the x and y derivatives of z_s are given:

$$\frac{\partial z_s}{\partial x} = \frac{1}{\rho g H} \left[\frac{\partial}{\partial x} \left(2\nu H \left(2\frac{\partial u_d}{\partial x} + \frac{\partial v_d}{\partial y} \right) \right) + \frac{\partial}{\partial y} \left(\nu H \left(\frac{\partial u_d}{\partial y} + \frac{\partial v_d}{\partial x} \right) \right) - \beta^2 u_d \right] \quad (12)$$

and,

$$\frac{\partial z_s}{\partial y} = \frac{1}{\rho g H} \left[\frac{\partial}{\partial y} \left(2\nu H \left(2\frac{\partial v_d}{\partial y} + \frac{\partial u_d}{\partial x} \right) \right) + \frac{\partial}{\partial x} \left(\nu H \left(\frac{\partial u_d}{\partial y} + \frac{\partial v_d}{\partial x} \right) \right) - \beta^2 v_d \right] \quad (13)$$

A necessary condition for the gradient of any scalar field is that its curl be zero:

$$\nabla \times \nabla z_s = 0 \quad (14)$$

Observe that this property of the surface elevation gradient has been referred to previously to suggest that the driving stress cannot be as efficient as basal friction in producing the observed curl of the velocity.

It is not possible in practical situations to ensure that the velocity observations, when substituted into (12) and (13) with uniform β , would satisfy (14). As a result, the inverse problem is best solved using control methods. I define the performance index J in the same manner as before but regard $z(x,y)$ rather than $\beta(x,y)$ as the unknown. As with the treatment of β , z_s is expanded in terms of the functions which possess spatial scales appropriate to the resolution of the velocity observations:

$$z_s(x,y) = \sum_{i=1}^{903} \zeta_i F_i(x,y) \quad (15)$$

The expression for $\partial J / \partial \zeta_i$ is

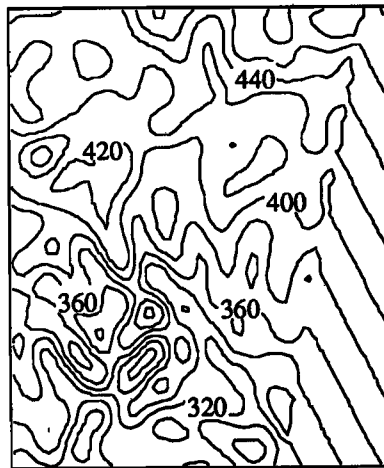
$$\frac{\partial J}{\partial \zeta_i} = \iint_{\Gamma} -\rho g H \left(\lambda \frac{\partial F_i}{\partial x} + \mu \frac{\partial F_i}{\partial y} \right) dx dy \quad (16)$$

The condition for minimization of J is

$$\frac{\partial J}{\partial \zeta_i} = 0 \quad (17)$$

Following the same technique used to satisfy $\partial J / \partial \alpha_1 = 0$ in the inference of β , I satisfied (17) under the assumption of a constant $\beta = 3.7 \times 10^4 \text{ (Pa s/m)}^{1/2}$ within the interior of the ice stream. (Over the exterior, β is augmented by the amount discussed previously to reproduce the stagnant conditions there.) This constant was chosen so that the average of the basal friction over the interior of the ice stream would be approximately the same as in Figure 8. The inferred z field is shown in Figure 11 and can be compared with the surface elevation interpolated from *Drewry's* [1983] maps in Figure 3. Mismatch between the observed and modeled velocity in this instance was significantly greater than that encountered in the inversion for β (Figure 12).

The inferred z displays small-scale surface undulations having amplitude and wavelength that are typical for ice streams (Figure 11). The linear series of bumps and depressions that emanates from the ice stream edge, as seen in the Landsat image (Figure 1a), is not apparent in the inferred surface elevation. To further examine this lack of



surface elevation (m)

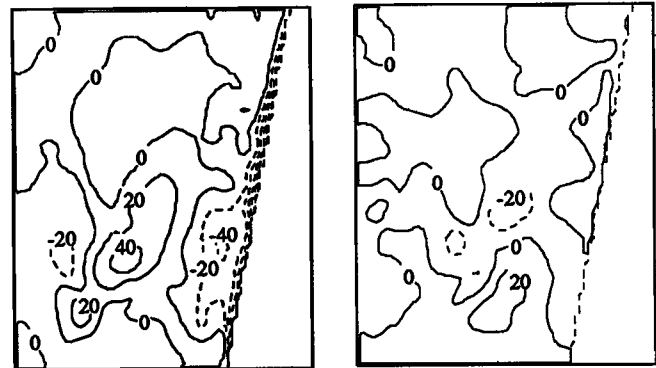
Fig. 11. Contour map of the inferred surface elevation generated from the velocity data under the assumption of a uniform basal friction coefficient ($\beta = 3.7 \times 10^4 \text{ (Pa s/m)}^{1/2}$).

correspondence, I constructed a synthetic Landsat image, shown in Figure 13. I assigned a gray-scale value to each grid cell in the finite difference representation of z according to the cosine of the angle between a perpendicular to the free surface and the incoming solar radiation. The solar elevation and azimuth were taken to be the same as when the Landsat image in Figure 1a was acquired (18° and 105° , respectively). A low-pass filtered copy of the Landsat image in Figure 1a is also shown in Figure 13 for comparison.

Visual comparison of the filtered Landsat image with its synthetic counterpart shows that the inferred z could not be exactly the same as the real surface elevation. I was unable, however, to quantify this difference because I did not have the necessary digital Landsat image information. The qualitative visual difference, nevertheless, suggests that a spatially constant β is not likely. To the extent that surface elevation alone is unable to explain the observed surface velocity, a spatially variable basal friction appears to be confirmed.

CONCLUSION

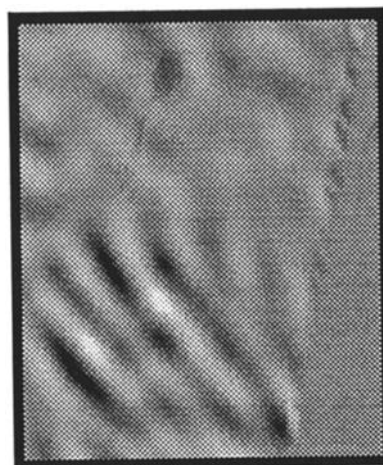
In this study, I have used control methods to infer basal friction from an observed surface velocity pattern of ice stream



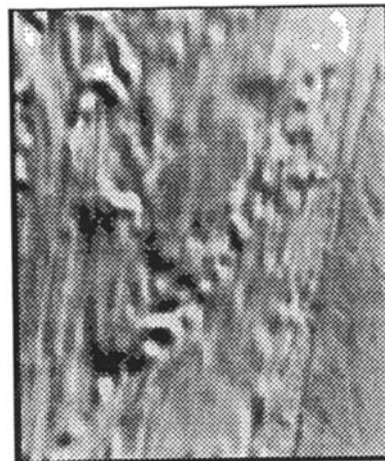
longitudinal velocity misfit (m/yr)

transverse velocity misfit (m/yr)

Fig. 12. $U - U_0$ associated with the z field shown in Figure 11 and uniform β . This difference can be compared with that in Figure 7 and suggests that surface undulations alone cannot explain the major variations in observed velocity.



simulated LANDSAT image



LANDSAT image (low pass filtered)

Fig. 13. Simulated Landsat gray-scale image derived from the inferred surface elevation (left). Low-pass filtered version of the Landsat image shown in Figure 1a (right).

E. The significance of the inferred distribution is that it provides a well-resolved characterization of the subglacial bed that can be used to test theories concerning its hydrological and mechanical properties. An initial analysis of the basal friction suggests that it is not related to the local ice stream velocity. This conclusion argues against the existence of a uniform layer of deformable subglacial sediment of constant viscosity. Zones of exceedingly high basal friction, where the basal shear stress approaches 10^5 Pa, appear to correlate with surface undulations visible in Landsat imagery. This suggests that the rigid bedrock substratum may influence lubricating qualities of a deformable subglacial till, if indeed such a till exists.

The inferred basal stress variation is confirmed by the fact that basal friction alone can have a curl of sufficient magnitude to explain the curl of the observed velocity field. Driving stress, which is the largest source of uncertainty, cannot reproduce the effects of the basal stress variation because the curl of a driving stress in general is a second-order quantity. To further refine the derived basal friction distribution, however, additional measurements of the ice thickness and surface elevation are needed. These measurements can be conducted by remote sensing (aircraft radar for thickness, satellite altimetry for surface elevation); thus the prospects for characterizing the dynamic controls on ice stream E are quite good.

As demonstrated here, control methods provide an efficient algorithm for inverting the velocity observations for the basal friction. The precision with which a modeled velocity was fit to the observed velocity serves as a confirmation of the ice stream dynamics used here and of the benefits of using control methods in conjunction with models. Control methods thus offer a means to better integrate the two most common research activities in glaciology: modeling and field observation.

NOTATION

Λ	Lagrange multiplier vector, $(\text{Pa s}^2/\text{m}^2)^{-1}$.
α_i	coefficients of the series expansion for β .
β	basal friction parameter, $(\text{Pa s}/\text{m})^{1/2}$.
B	flow law parameter, $\text{Pa s}^{-1/n}$.
F_i	basis functions for the expansion of β and z_s .
g	gravitational acceleration, m/s^2 .
H	ice thickness, m.
J	performance index, m^2/s^2 .
λ	Lagrange multiplier component, $(\text{Pa s}^2/\text{m}^2)^{-1}$.
μ	Lagrange multiplier component, $(\text{Pa s}^2/\text{m}^2)^{-1}$.
ν	effective viscosity, Pa s.
n	flow law parameter, nondimensional.
ρ	ice density, kg/m^3 .
Σ	uncertainty weighting function, nondimensional.
u	horizontal velocity, m/s.
v	horizontal velocity, m/s.
x	horizontal coordinate, m.
y	horizontal coordinate, m.

z_b	basal elevation, m.
z_s	surface elevation, m.
ζ_i^s	unknown coefficients of the series expansion for z_s .

Acknowledgments. Financial support was provided by NSF grant DPP 89-14938 to the University of Chicago. Computer support was provided by the National Center for Atmospheric Research. I thank Robert Bindschadler and Ted Scambos for providing assistance with the research. Kolumban Hutter and Carlisle Thacker reviewed a manuscript on a similar subject and provided helpful suggestions. Richard Alley, John Firestone, Richard Frolich, Miriam Jackson, Kees Van der Veen, Ed Waddington, Ian Whillans, and an anonymous referee are also thanked for their help.

REFERENCES

- Alley, R. B., D. D. Blankenship, C. R. Bentley, and S. T. Rooney, Till beneath ice stream B, 3, Till deformation: Evidence and implications, *J. Geophys. Res.*, 92(B9), 8921-8929, 1987.
- Balise, M. J., and C. F. Raymond, Transfer of basal sliding variations to the surface of a linearly viscous glacier, *J. Glaciol.*, 31(109), 308-318, 1985.
- Bindschadler, R. A., and T. A. Scambos, Satellite-image-derived velocity field of an Antarctic Ice Stream, *Science*, 252(5003), 242-246, 1991.
- Bindschadler, R. A., S. N. Stephenson, D. R. MacAyeal, and S. Shabtaie, Ice dynamics at the mouth of ice stream B, Antarctica, *J. Geophys. Res.*, 92(B9), 8885-8894, 1987.
- Bryson, A. E., Jr., and Y. C. Ho, *Applied Optimal Control: Optimization, Estimation and Control*, 481 pp., John Wiley, New York, 1975.
- Drewry, D. J., (Ed.), *Antarctica: glaciological and geophysical folio*, scale 1:6,000,000 Univ. of Cambridge, Scott Polar Res. Inst., Cambridge, England, 1983.
- Engelhardt, H., N. Humphrey, B. Kamb, and M. Fahnestock, Physical conditions at the base of a fast moving Antarctic ice stream, *Science*, 248(4951), 57-59, 1990.
- Frolich, R. M., and C. S. M. Doake, Relative importance of lateral and vertical shear on Rutford Ice Stream, Antarctica, *Ann. Glaciol.*, 11, 19-22, 1988.
- MacAyeal, D. R., Large-scale ice flow over a viscous basal sediment: Theory and application to Ice Stream B, Antarctica, *J. Geophys. Res.*, 94(B4), 4071-4087, 1989.
- Stephenson, S. N., and R. A. Bindschadler, Is ice-stream evolution revealed by satellite imagery?, *Ann. Glaciol.*, 14, 271-277, 1990.
- Thacker, W. C., and R. B. Long, Fitting dynamics to data, *J. Geophys. Res.*, 93(C2), 1227-1240, 1988.
- Thomas, R. H., and D. R. MacAyeal, Derived characteristics of the Ross Ice Shelf, Antarctica, *J. Glaciol.*, 28(100), 397-412, 1982.
- Whillans, I. M., Y-H. Chen, C. J. Van der Veen, and T. J. Hughes, Force budget: III. Application to three-dimensional flow of Byrd Glacier, Antarctica, *J. Glaciol.*, 35(119), 68-80, 1989.
- Wunsch, C., Transient tracers as a problem in control theory, *J. Geophys. Res.*, 93(C7), 8099-8110, 1988.

D. R. MacAyeal, Department of Geophysical Sciences, University of Chicago, 5734 South Ellis Avenue, Chicago, IL 60637.

(Received April 3, 1991;
revised August 23, 1991;
accepted September 19, 1991.)